Estimation of Discharge Coefficients for Free-Flowing Compound Weirs with Upstream Horizontal Flow Contraction

Yildiz, Burhan; Uijttewaal, Wim S.J.

DOI
10.1061/JHEND8.HYENG-14133

Publication date
2025

Document Version
Final published version

Published in
Journal of Hydraulic Engineering

Estimation of Discharge Coefficients for Free-Flowing Compound Weirs with Upstream Horizontal Flow Contraction

Burhan Yildiz, Ph.D.[1]; and Wim S. J. Uijttewaal, Ph.D.[2]

Abstract: Compound weirs have been used as adjustable structures to divert flow, for example, through river branches at the river bifurcations. For this purpose, a wide variety of weir configurations can be used including asymmetric configurations that have not been studied in the literature yet. A proper one-dimensional representation of flow over these structures is needed as the effect they have on the river are generally added as subgrid energy losses to the river hydrodynamic models. In this study, an experimental study was conducted to estimate the correct representation of compound weirs at varying weir configurations and flow conditions. In the experimental campaign, eight weir configurations were used with six discharge values. Upstream flow depths at each case were recorded and their relationship with the flow rate and weir configuration was analyzed. A 1D model was proposed to estimate flow rates when the upstream flow depths are known. The proposed correction to the well-known Kindsvater and Carter approach was applied to modify the discharge coefficient when nonuniform geometries are used that cause horizontal flow contraction. To estimate and validate the proposed correction, additional numerical simulations using computational fluid dynamics (CFD) were conducted to estimate the detailed flow field upstream of the nonuniform weirs. Surface particle image velocimetry (SPIV) measurements were also conducted to validate the CFD model. The corrected 1D model predicted the flow rates at 48 cases covering uniform to highly nonuniform weir geometries with a maximum of 9.7% and a mean of 2.45% deviation from the measurements. Additional tests on the performance of the proposed model validated its effectiveness in various nonuniform geometries at low flows. However, when substantial changes are made to the geometry, such as the removal of buttresses, the model may require calibration to maintain its accuracy. **DOI: 10.1061/JHEND8.HYENG-14133.** *© 2025 American Society of Civil Engineers.*

Practical Applications: Compound weirs are used at the river bifurcations to add resistance to one side of the branch and distribute the flow according to the needs of the people. Defining the flow rate as a function of the flow depth by using one-dimensional formulas would help engineers to accurately model the river behavior. However, in compound weirs, flow can become two-dimensional if nonuniform weir geometries were used and then mass was transported in the lateral direction. The 1D weir formulas that exist in the literature are incapable of defining the effect of lateral flow on the flow rate passing over a weir. In this study, a 1D model was developed that includes the effect of lateral flow and quantified it with a new parameter that can be calculated by using the variance of flow rates over each weir notch. The model was tested and validated using physical experiments and three-dimensional numerical model tests.

Author keywords: Diversion structures; Compound weir; Sharp-crested weir; Rectangular weir; Free-flowing weir; Experimental hydraulics; Numerical model; Computational fluid dynamics (CFD); Surface particle image velocimetry (SPIV); k-ω shear stress transport (SST) turbulence model.

Introduction

Various kinds of weirs have been used in open channels for flow rate measurement, flow regulation, or flow diversion (Emiroglu et al. 2010; Ferdowsi et al. 2021; Clemmens et al. 2001). Weirs are categorized based on their cross-sectional shapes, like rectangular, triangular, or cylindrical weirs, as well as their lengths in the flow direction as sharp- or broad-crested weirs. Also, if the normal direction of the weir aligns with the flow direction they are termed frontal weirs. Weirs can also be categorized based on their downstream effect as either submerged or free-flowing, depending on whether the water level downstream of the weir is below or above the crest of the weir, respectively. In free-flowing weirs, the flow becomes supercritical after passing the weir, while it was subcritical upstream. Estimating the flow rate equation for a weir is important for the use of them in flow diversion and measurements. The existing equations are working well for the free flow over simply shaped frontal weirs. When deriving the one-dimensional formula for sharp-crested weirs, the pressure over the weir is assumed to be atmospheric and the energy loss upstream is neglected (Rehbock 1929; Henderson 1966; Bos 1989). The following equation is for the flow rate Q for rectangular sharp-crested free-flowing weirs (Kindsvater and Carter 1957):

$$Q = \frac{2}{3} b_e C_d \sqrt{2g} h_e^{\frac{3}{2}} \tag{1}$$

[1]Assistant Professor, Dept. of Civil Engineering, Mugla Sitki Kocman Univ., Mugla 48050, Türkiye; Researcher, Dept. of Hydraulic Engineering, Delft Univ. of Technology, Delft 2628 CN, Netherlands; currently, Postdoctoral Research Associate, Dept. of Civil and Environmental Engineering, Univ. of Liverpool, Liverpool L69 3GQ, UK (corresponding author). ORCID: https://orcid.org/0000-0002-0144-3562. Email: burhanyildiz@mu.edu.tr

[2]Professor, Dept. of Hydraulic Engineering, Delft Univ. of Technology, Delft 2628 CN, Netherlands. ORCID: https://orcid.org/0000-0002-6043-8026. Email: w.s.j.uijttewaal@tudelft.nl

Note. This manuscript was submitted on March 13, 2024; approved on December 24, 2024; published online on March 27, 2025. Discussion period open until August 27, 2025; separate discussions must be submitted for individual papers. This paper is part of the ***Journal of Hydraulic Engineering***, © ASCE, ISSN 0733-9429.

where b_e is the effective width of the weir; C_d is the weir coefficient; g is the gravitational acceleration; and h_e is the effective upstream flow depth. The effective weir width and effective flow depth includes the effects of viscosity and surface tension. b_e was defined as $b_e = b + K_b$, where b is the width of the weir and K_b changes between +4.3 mm to −1 mm depending on the end contraction. h_e was defined as $h_e = h_0 + K_h$, where h_0 is the upstream flow depth referencing the weir crest level and K_h equals 1 mm. The weir coefficient, C_d, includes the neglected effects like the energy losses and velocity head upstream. It was empirically defined by many researchers, including Rehbock (1929) and Swamee (1988). Kindsvater and Carter (1957) defined it as a function of the end contraction (ratio of the weir width b to approach channel width B). When there is no end contraction, the equation is as follows:

$$C_d = 0.602 + 0.075\left(\frac{h_0}{P}\right) \tag{2}$$

where P is the weir height. The effect of end contractions was applied by decreasing the right-hand-side coefficients of Eq. (2) accordingly. For example, when $b/B = 0.9$, the equation becomes $C_d = 0.599 + 0.064(h_0/P)$. Recent studies have sought proper representations of flow at various types of weirs, including compound weirs. Compound weirs are composed of several weir sections that can be adapted to distribute or divert the flow. They have been widely used for discharge measurement particularly to mitigate measurement errors associated with low water levels. The 1D representation of flow through compound weirs was achieved mainly by using two main methods. In the first method, the researchers assumed the compound section of the weir as a single section and defined the relevant sectional properties for the entire geometry. These parameters were used as the sectional properties in the derivation of Eq. (1). Göğüş et al. (2006), Al-Khatib and Gogus (2014), and Zhao et al. (2015) applied this method successfully to broad-crested compound weirs composed of three sections. However, this method is not applicable in cases where buttresses separate the compound weir notches or in instances of highly asymmetric or highly nonuniform geometries. In the second method, researchers treated the weir notches as individually working elements. They applied 1D weir formulas like Eq. (1) to each notch and estimated the discharge capacity of the weir by superposing the estimates from each notch. Jan et al. (2009) and Kulkarni and Hinge (2020) used this method at broad-crested weirs. Martinez et al. (2005), Jan et al. (2006), Piratheepan et al. (2006), and Lee et al. (2012) applied it for sharp-crested weirs composed of two or three individual elements. This method is particularly suitable for weirs with buttresses.

In addition to 1D models, soft computing methods such as artificial neural networks or genetic programming are employed to predict discharge coefficients (Salmasi et al. 2013; Li et al. 2021; Nouri et al. 2023). Furthermore, Zahiri et al. (2014) employed a two-dimensional method based on depth-averaged Navier-Stokes equations, supplemented by calibration parameters to enhance solution accuracy. For a more proper representation of flow field over the weirs, more comprehensive numerical methods were preferred by the researchers. Qu et al. (2009) employed a computational fluid dynamics (CFD) application with a 2D vertical mesh to model flow over a rectangular sharp-crested weir without lateral variation. In cases where the weir section exhibits lateral variation, three-dimensional meshes were selected, and the results were effectively validated using either experimental data or analytical solutions (Savage et al. 2016; Altan-Sakarya et al. 2020; Torres et al. 2021; Yildiz et al. 2021).

Compound weirs serve not only as efficient instruments for measuring flow rates, where merely two or three segments suffice, but also as versatile tools for flow diversion, a task for which their notch count may exceed twenty. Figs. 1(a and b) show a compound weir located at the right bank flood plain of the Nederrijn (a branch of Dutch Rhine River) bifurcation in the Netherlands to divert flow through branches. Buttresses are commonly employed in this kind of large weir design between weir notches due to operational considerations. The presence of buttresses also facilitates the straightening of flow before it reaches the weir crest, thereby reducing lateral flow over the crest (Wessels and Rooseboom 2009). The compound weirs are designed to add discharge- (or stage-) dependent resistance to one side of the bifurcation. For this purpose, they can be operated in asymmetric or nonuniform configuration. Nonuniform configurations of the weir can induce horizontal flow contraction and lateral flow over the crest, eventually impacting its capacity. The horizontal flow contraction is commonly observed in the operation of controlled spillways and open check dams in hydraulic engineering. Operators aim to direct high discharges away from the banks to prevent erosion and maximize conveyance capacity. This often results in nonuniform flow patterns and horizontal flow contraction. Characterizing this issue by using a 1D model poses considerable challenges. The initiation of pronounced lateral flow can be attributed to variations in weir crest elevations among adjacent notches. Additionally, the discharge capacity of a notch can easily be influenced by the condition of another notch further away from it. Employing 1D formulas to define compound weirs is essential in river hydrodynamic modeling tasks. Integrating compound weirs into numerical hydrodynamic models necessitates a fine mesh to accurately represent their geometry. Yet, river hydrodynamic models often utilize coarse meshes, leading to

Fig. 1. (a) Aerial view of the compound weir located at the right bank flood plain of the Pannerden bifurcation in the Netherlands (image courtesy of Rijkswaterstaat, The Netherlands); and (b) the compound weir closer view from upstream, Rijnwaardense Uiterwaarden (n.d.) (image courtesy of Marc Pluim).

the incorporation of these structures' effects as subgrid energy losses (Yildiz et al. 2024). Consequently, a representative loss term tailored to these structures becomes essential. To date, no study in the Web of Science database addresses flow analysis over complexly shaped compound weirs.

In this study, an experimental campaign was set up to analyze flow over compound weirs with buttresses encompassing a diverse array of configurations ranging from uniform to nonuniform and asymmetric ones. The aim is to understand the mechanisms underlying energy losses and to develop and validate a predictive 1D model. The basis of the model is established by treating the flow over each weir notch individually. The well-known Kindsvater and Carter approach [Eq. (1)] is employed in this study, with certain modifications to accommodate the presence of buttresses and empty weir gates. The free surface level over the crests of each notch was not assumed to be constant. Additionally, we did not estimate the flow depths over the crests, as this would require additional assumptions regarding head loss terms. To investigate the flow behavior further and validate the 1D model, CFD models are developed with 3D meshes. The Reynolds-averaged Navier–Stokes (RANS) modeling technique is selected, coupled with a k-ω shear stress transport (SST) turbulence closure. Moreover, surface particle image velocimetry (SPIV) is employed in this study to capture surface velocities in a selected case, facilitating their utilization in the validation process of the numerical model. Utilizing insights from both the 1D analytical model and the CFD simulations, this study proposes a correction to the discharge coefficients tailored for nonuniform weir geometries. This correction demonstrates efficacy across all tested cases, enhancing the accuracy of discharge predictions.

Experimental Method

The experiments were conducted in a 20-m-long rectangular horizontal flume with a 3-m-wide smooth bed and 0.25-m-high steel side walls at the Hydraulic Engineering Laboratory of Delft University of Technology, Netherlands [Figs. 2(a and b)]. An adjustable compound weir model with 12 rectangular notches (openings) was used, which can be considered as a 1:25 schematized, geometrically scaled model of the prototype of Fig. 1(b). Each weir notch had a width of 23 cm with 2-cm-thick wooden buttresses between them [Fig. 2(a)]. The weir structure was formed by using 2-mm-thick steel plates leading to a sharp-crested weir at every flow condition. The weir was in the middle of the flume, i.e., 10 m away from the inlet [Fig. 2(b)]. The subcritical flow was straightened by a honeycomb before entering the flume and the surface water waves were dampened by a 1-m-long rectangular foam block located at the free surface at the inlet. It was 9 m (around 45 times the maximum flow depth) away from the weir crest, which was found as a safe distance to dissipate the external effects of it on the flow. Eight compound weir configurations were selected, and each was tested for six discharge values ranging from 20 L/s to 70 L/s with 10-L/s increments. The weir dimensions are given in Fig. 3 in graphical form and in Table S1 in the Supplemental Materials in tabular form. The threshold amounts to the weir footings, which are around 3 mm, were added to the numerical values in Table S1. The configurations were selected to include flow variety and to cover a wide range of applications. Some configurations were selected uniform (C2 and C3), some were selected as symmetric and non-uniform (C5, C7, and C9), and some were selected as asymmetric leading to weak (C4 and C6) and

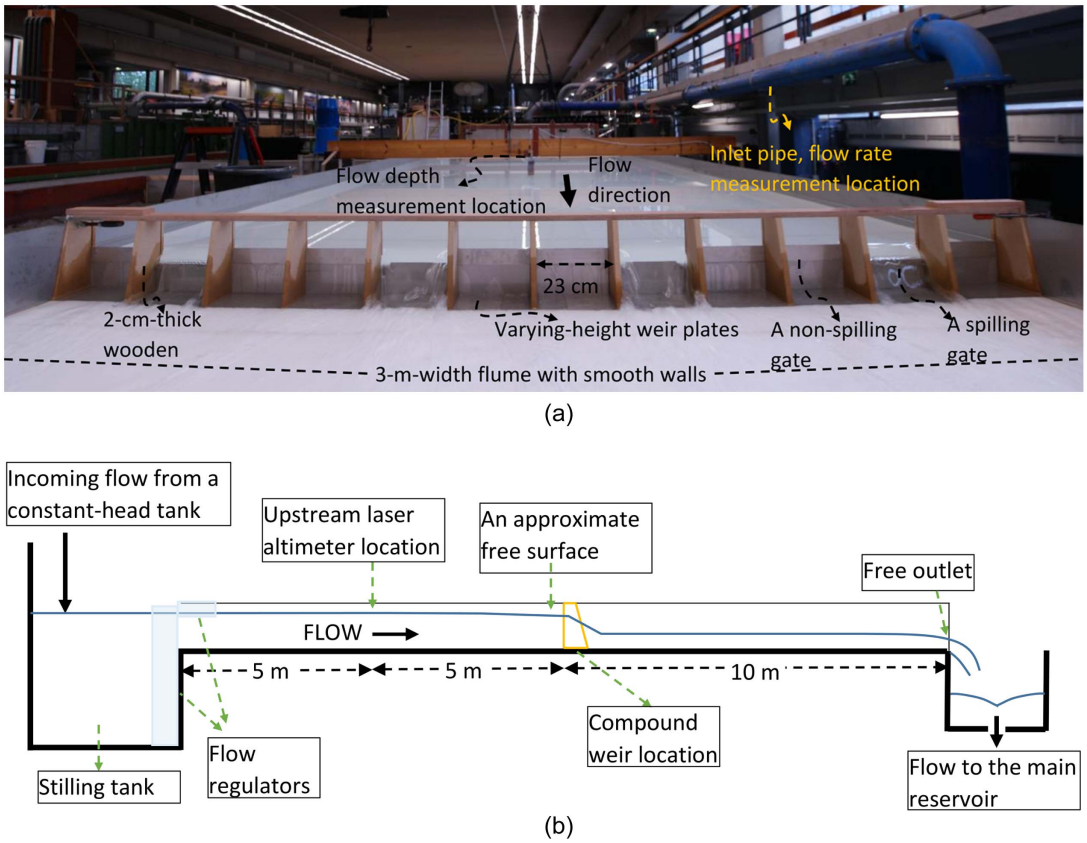

Fig. 2. (a) The flume with a compound weir model (C5) installed when a discharge of $Q = 20$ L/s was flowing in it; and (b) schematic diagram of the flume (not to scale).

J. Hydraul. Eng., 2025, 151(4): 04025013

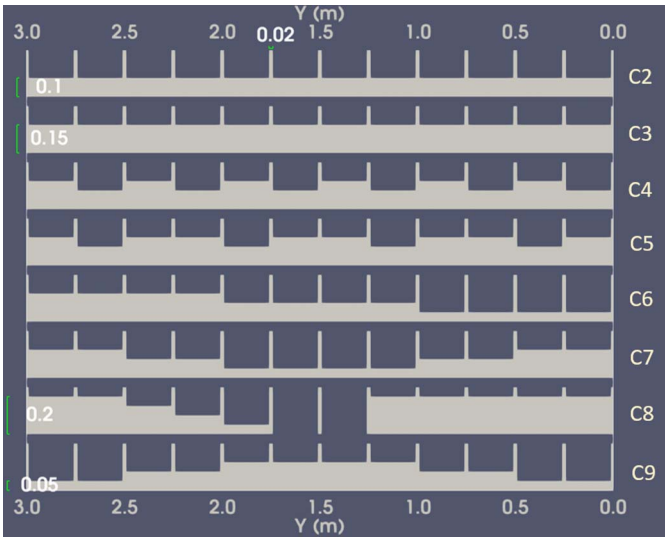

Fig. 3. Tested weir geometries in the experiments (all dimensions in m, the dimensions exclude the thresholds at each gate, which are approximately 3 mm each, see Table S1 in the Supplemental Materials for tabular data).

to strong (C8) horizontal flow contractions. During data recording, the flume tail gate was fully open to have free flow there. Steady discharges were obtained and checked by instantaneous flow rate measurements. The discharges were recorded by using an acoustic flowmeter at the inlet pipe. Water depth levels were recorded by using a laser altimeter located 5 m upstream of the weir. The uncertainty analysis and the associated errors are provided as Supplemental Materials. Furthermore, SPIV measurements were carried out at the same flume using configuration C8 at 70 L/s to use them in the validation of the numerical model. A camera was mounted over the flume with its camera angle covering the whole width and extending up to 3 m upstream of the weir. Tracer particles were disposed at the inlet of the flume and their instantaneous positions were recorded by taking pictures. The processing of the data was done using the PIVLab tool of Matlab (Thielicke and Sonntag 2021). The uncertainties in the SPIV results may be attributed to image processing settings, given that the flow was considered steady based on simultaneous measurements of instantaneous flow depth and flow rate. Trials with a limited number of applicable image processing settings resulted in a maximum deviation of 3% in the mean velocities, which we assumed as the estimated error.

1D Analytical Model

In the 1D model, the flow rates passing through each weir notch were estimated separately by using Eq. (1). The viscosity and surface tension correction for effective weir width estimation (K_b) was proposed by Kindsvater and Carter (1957), assuming the end contraction is developed with two extensions on both sides of the flume. However, in this study, the contraction was formed by using short buttresses, which develop an end contraction without the existence of side walls. Therefore, the friction to be added by the side walls is missing. This leads to higher velocities and, thus, higher discharges at each weir notch. In our model, the K_b value was calibrated by testing the convergence of the uniform configurations (C2 and C3), and it was increased from the originally suggested 0.35 cm to 1.5 cm. The correction for effective upstream flow depth, K_h, used was 1 mm, as suggested by Kindsvater and Carter (1957).

Bos (1989) suggested that the h_0/P ratio (where P is the weir height) should be less than 5 to maintain the effectiveness of rectangular sharp-crested weirs as control structures. For weir plates that did not meet this criterion—specifically, the empty gates used in configurations C8, C11, and C12—we treated them as broad-crested rectangular weirs. This was based on the presence of approximately 3-mm-high, 15-cm-long threshold plates at the weir section. Following the recommendations of Bos (1989) and Sargison and Percy (2009), we used a weir coefficient of 0.66 for these empty gates, adapting their suggested coefficients to the formula used in this study [Eq. (1)]. This adjustment led to the convergence of the 1D model results for configuration C8 after the proposed correction was applied. Weir coefficients for the rest were estimated by using Eq. (3), which is obtained by interpolating the coefficients of Eq. (2), as suggested by Kindsvater and Carter (1957) for the end contraction due to the added buttresses ($b/B = 0.92$):

$$C_d = 0.6 + 0.066\left(\frac{h_0}{P}\right) \tag{3}$$

Then, the total discharge was estimated at each case as the summation of the ones obtained at each notch. There were nonflowing weir notches in some cases. This condition was checked in the model with $h_0 \geq P$ condition to be held true for the flowing notches. The water levels can vary from the flow depth measurement location to the weir section due to vertical flow contraction, energy losses, or stagnation pressures at the boundaries. However, this variation was necessarily neglected in the analytical model. In order to include the physics related to horizontal contraction and stagnation pressures, a more detailed analysis needs to be performed using a 3D approach.

3D CFD Model

The numerical setup was prepared for the nonuniform configurations (C4 to C9). They were prepared and executed by using the interFoam solver of the OpenFOAM-v2006 (OpenCFD, n.d.) software. interFoam is an incompressible multiphase solver that uses the volume of fluid method (Hirt and Nichols 1981) to handle multiphase flow. It uses a finite volume approach to solve for the incompressible continuity and RANS equations. It includes the effect of surface tension at the interfacing cells. The model equations are as follows:

$$\frac{\partial u_i}{\partial x_i} = 0 \tag{4}$$

$$\frac{\partial(\rho u_i)}{\partial t} + \frac{\partial(\rho u_i u_j)}{\partial x_j} = -\frac{\partial p}{\partial x_i} + \frac{\partial}{\partial x_j}\left(\mu\frac{\partial u_i}{\partial x_j} - \rho\overline{u_i' u_j'}\right) + \rho g_i + T\kappa\frac{\partial \alpha}{\partial x_i} \tag{5}$$

where u_i is the time-averaged velocity in direction x_i; ρ is the density; p is the pressure; μ is the molecular viscosity; and $\rho\overline{u_i' u_j'}$ is the Reynolds stress term. The last term on the right adds the effect of surface tension, with T denoting the surface tension with a magnitude 0.07 N/m for air–water contact surfaces. The interface curvature is denoted by κ and α is the volume fraction of water in the computational cell. The density at each cell is defined by using the volume fraction of water and air phases as follows:

$$\rho = \alpha\rho_{\text{water}} + (1-\alpha)\rho_{\text{air}} \tag{6}$$

The molecular viscosity at each cell is defined similarly using air and water viscosities. An additional advection equation is written for the conservation of volume fraction term, α, as follows:

$$\frac{\partial \alpha}{\partial t} + \frac{\partial (\alpha u_i)}{\partial x_i} + \frac{\partial}{\partial x_i}(\alpha(1-\alpha)u_i^r) = 0 \tag{7}$$

where u_i^r is defined as the modeled relative velocity, which is meant to give the difference between phase velocities (Okagaki et al. 2021). The third term is added to preserve the surface sharpness by compressing the interface following the multidimensional universal limiter with explicit solution (MULES) algorithm. The Reynolds stress term in Eq. (5) was modeled using the eddy viscosity concept (Boussinesq 1877) and k-ω SST turbulence model (Esch and Menter 2001; Menter et al. 2003), which uses standard k-ω turbulence model near wall zones and standard k-ε turbulence model away from the wall zones (k: turbulent kinetic energy, ω: specific rate of turbulent dissipation, and ε: rate of dissipation of k). This method was found to be successful in solving the flow separation (Versteeg 2007; Jiang et al. 2018).

The principles in determining the dimensions of the flow domain are given as follows. The longitudinal distance from the inlet to the weir was used as the same with the physical experiments (10 m). The longitudinal distance from the weir to the outlet was selected as short (0.5 m), considering that the flow is supercritical after passing the weir, which would have no impact on the flow over the weir. It was later validated that this length was sufficient as the flow there does not disturb the flow over the weir. The lateral dimension of the domain was selected the same as the flume width of the experiments. When the inlet discharge was 70 L/s, the height of the domain was selected as 0.30 m, which was found to be a safe height considering the highest measured flow depth was 0.205 m in the experiments. The height of the domain was adapted accordingly for the other tested discharge values.

The computational mesh for each case was generated by first forming a structured background mesh covering the whole flume using hexahedral elements. In the longitudinal direction, the mesh was refined gradually starting from the inlet. We observed that the streamlines start to curve on the surface around 1.5 m to 2 m from the weir at the most extreme case. Therefore, to increase the accuracy in that region a fine mesh was used for each case starting from 1.8 m upstream from the weir up to the weir itself. In the vertical direction, refinement was applied around the expected free surface location for a better convergence in the flow depth prediction. The number of computational points in the z-direction (n_z) were tested from 10 to 40 to assess the dependence of the results to the mesh. The chosen alternative was further tested by comparing its results with two meshes that had the same number of computational points in the vertical direction but different levels of refinement in the horizontal direction. The weir geometry files were developed separately, and they were included in the domain by applying additional refinement around them to represent the geometry well in the mesh. This was achieved by using the snappyHexMesh utility of OpenFOAM. This strategy resulted in around 1×10^6 computational cells at each case. Views of the developed computational mesh for the C4 case are given in Fig. 4. We employed an adjustable time step in the simulations, enabling its reduction as necessary to comply with the chosen maximum Courant number value of 0.5.

The inlet boundary condition of the model was defined as the specified volumetric flow rate with varying flow depth [variableHeightFlowRateInletVelocity boundary condition for velocity (U) in OpenFOAM], considering that it would reflect the physical reality best. At the outlet, the gradients of the velocity and pressure were defined as zero with a stopper for adverse flow [inletOutlet boundary condition for U, zeroGradient boundary condition for pressure term (p_rgh) in OpenFOAM]. Side and bottom solid boundaries were selected as no-slip smooth walls. Near-wall treatment was applied by using a wall function [kqRWallFunction for k (turbulent kinetic energy) in OpenFOAM]. The top boundary condition was defined by an atmospheric pressure. An appropriate initial water volume with a velocity according to each case's measured data was defined for faster convergence. The simulations were run until the flow became steady, which took less than 100 s for almost all cases. When local velocities increased due to low weir gates, the free surface fluctuations at the beginning of the simulation also increased, leading to a longer convergence time. As a result, the C8 cases converged the slowest, with times for these simulations of 200 s.

Results and Discussion

Measured flow depths and discharge values are given in Yildiz and Uijttewaal (2023) and also in Table S2 in the Supplemental Materials. The configurations with larger blocking areas generally have a higher upstream depth h_u, when the tested discharges are the same. Only configuration C8 was excluded from this comparison. It had seven nonflowing notches at every tested flow rate. Therefore, the total blocking area cannot directly be estimated by superposing each weir plate height for C8. It was also expected to induce large horizontal flow contractions which makes it substantially different from the other configurations. Configurations C6, C7, and C9 have the same weir area and have almost the same h_u for the same discharge. Although having the same weir area as the previous three, C2 has larger h_u values. It has all the openings just overflowing while the others have low weirs with larger velocities. The comparison of the results with the 1D and CFD model results are given in the following section.

1D Analytical Model

The 1D model was applied as described earlier by having the upstream flow depth as the input and the flow rate as the output. The predicted flow rates were compared with the measured ones in Fig. 5. The model predictions at the uniform to slightly nonuniform cases (C2, C3, C4, and C5) are reasonably well. However, it substantially overestimates the data at four nonuniform configurations (C6, C7, C8, and C9). The overestimations are biggest for the C8 cases and moderate but very close for C6, C7, and C9. The flow over these heterogeneous configurations violated the 1D upstream flow conditions. The underestimation of the losses was linked with the significant transverse velocity component in the approach flow. Therefore, the 1D model was corrected by using the CFD model results, which is presented later in the "Proposed Correction for the 1D Model Discharge Coefficients" subsection.

3D CFD Model

Initially, the results of the alternative meshes were compared to ensure mesh independence. Eight mesh alternatives, varying in cell numbers across all three directions, were tested. These alternatives were evaluated based on streamwise and lateral velocities, as well as turbulent kinetic energy predictions at selected sections. Detailed information on this process is provided in the Supplemental Materials. The strategy used to develop the chosen mesh was then applied to the meshes for the remaining cases. When the tested discharge and, therefore, the simulated flow depths decreased, the

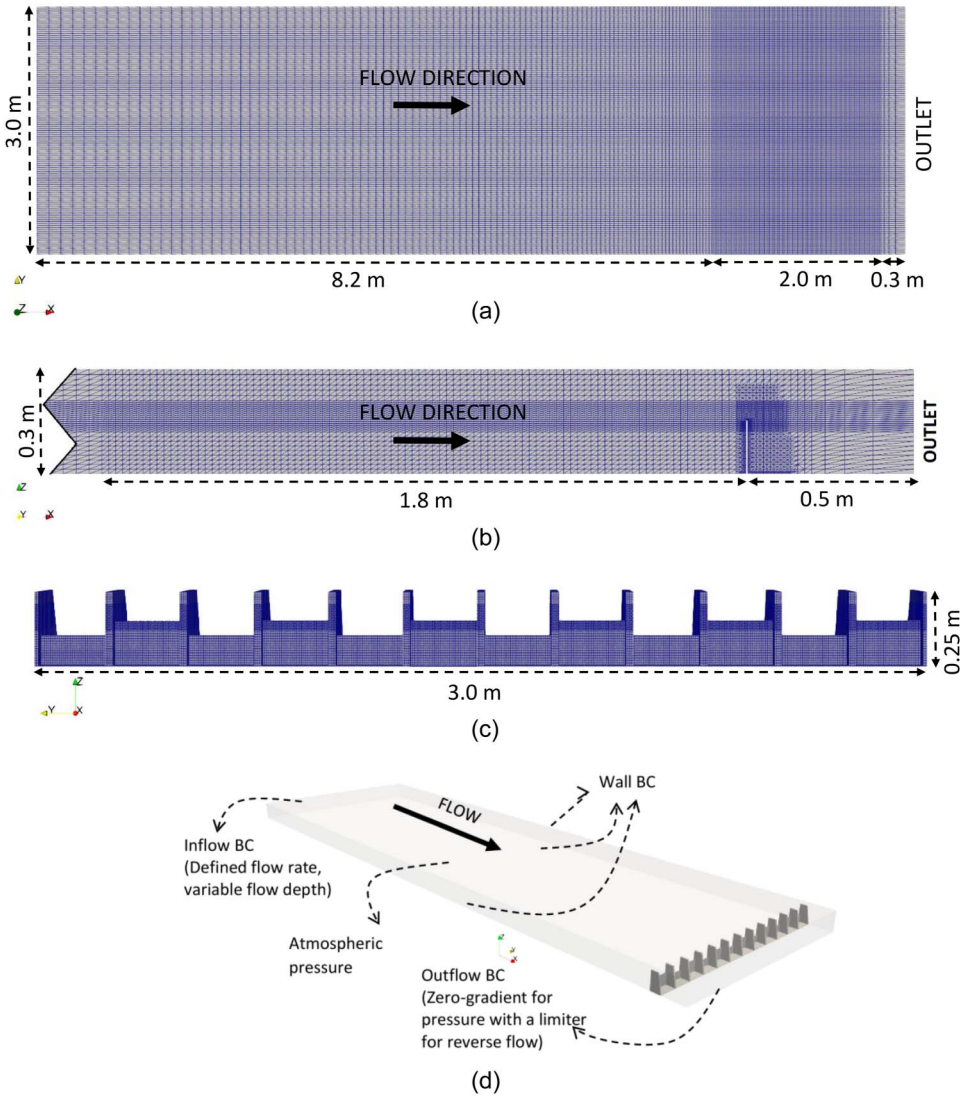

Fig. 4. The computational domain and the mesh as developed for configuration C4: (a) top view; (b) side view showing the part of the domain close to the weir ($n_z = 30$); (c) the weir structure with surface meshing; and (d) boundary conditions.

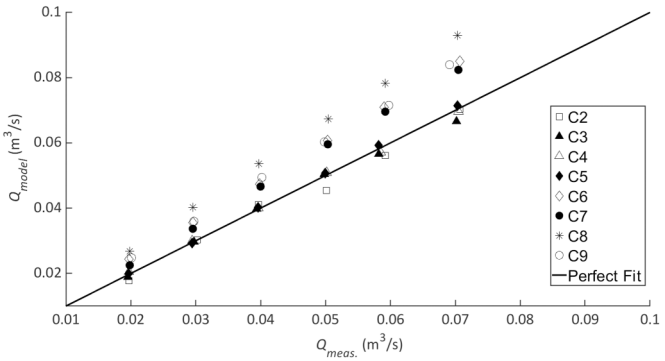

Fig. 5. Comparison of flow rates obtained from the uncorrected 1D analytical model and experimental data.

height of the flow domain was decreased to reduce the computational cost. In the development of the computational meshes of those cases, the same strategy was followed, i.e., if the domain height was 25 cm, the number of computational points in the z-direction was selected as 25 instead of 30 in the chosen mesh at which the domain height was 30 cm. Necessary adjustments were made in the distribution of the points to maintain the same strategy described. The meshes used in this study included between 900,000 to 1.1 million cells depending on the included weir geometry and domain height. The minimum cell size around the weir is 0.6 cm in the vertical and lateral directions and 0.2 cm in the streamwise direction. Due to varying flow conditions through the weir crests both within and between cases, the dimensionless wall distance, y^+ ($y^+ = (u_* y)/\nu$, where u^* is friction velocity estimated from the simulated wall shear stress values, y is distance from the center of the wall-neighboring cell to the nearest wall, and ν is the kinematic viscosity of water) differs at the weir crest. The simulation results indicated y^+ values were 80 at most portions of the weir crest in case C8Q70, while this value was 40 for case C4Q20. These two cases represent extreme scenarios regarding the developed velocity fields, suggesting that all other cases are expected to have y^+ values within these ranges.

The numerical model was simulated initially for 36 test cases considering configurations C4 to C9 and all tested discharges. The convergences of the inlet and outlet flow rates were tested.

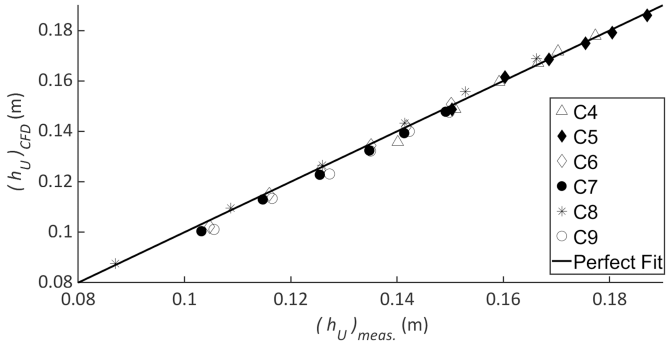

Fig. 6. Comparison of the upstream flow depths obtained from the CFD model and experimental data.

It was observed that they matched within a 1% error margin at each case tested. The water surface levels were estimated by labeling the levels with a water fraction of 0.5. The accuracy of the free surface determination depends also on the mesh resolution around that level. The comparison of the measured and the CFD-simulated upstream flow depths are given in Fig. 6 for each configuration. The percent relative error, ε, was estimated by using the following formula:

$$\varepsilon = 100 \times \frac{|(h_u)_{\text{model}} - (h_u)_{\text{measured}}|}{(h_u)_{\text{measured}}} \tag{8}$$

The predictions have 1.31% mean percent relative error with a maximum value of 4%. In order to have affordable computational meshes, and also considering that the main aim of the CFD simulations was to quantify the lateral flow contraction, the deviation in the flow depth predictions was regarded as allowable.

The horizontal flow constriction was observed in each scenario by examining the y-velocities, U_y, across the domain. Fig. 7 illustrates their variation across the free surfaces for two distinct cases, C8Q70 and C7Q20. The blank locations in both figures correspond to areas where the buttresses were removed from the figure to better visualize the isosurface behind them. In the C8 case, where the discharge is 70 L/s, the lateral velocity magnitudes immediately downstream of the buttresses surpass five times the approach velocity magnitude, indicating a concentration of discharge toward the sides. Additionally, when the lateral flow converges with the streamwise flow approaching the tip of a buttress, it deflects the streamlines, resulting in a reduction in the effective flow area at the weir. Despite the 6th and 7th gates of C8 having identical weir heights, stronger lateral flow is observed at the 7th gate, leading to a decrease in the flow area there. Specifically, the calculated flow area was 309.8 cm^2 for the 6th gate and 272.5 cm^2 for the 7th gate. However, the average x-velocity was higher at the 7th gate. The streamwise flow rate through the gates was determined by integrating the cell x-velocity over the area, resulting in estimates of 23.8 L/s for the 6th gate and 22.1 L/s for the 7th gate. This example underscores how neighboring weir heights influence the discharge passing through each gate. Moreover, it highlights that not only adjacent notches but sometimes notches three or four gates away can significantly impact the flow rate of a specific gate. In the C7 case depicted in Fig. 7, with a smaller discharge of 20 L/s and a less nonuniform configuration compared to C8, a similar effect is observed. Despite the four flowing gates having identical weir heights, the gates at the sides carry slightly less discharge due to exposure to higher lateral velocities, thereby reducing their effective flow area.

Fig. 8 shows the lateral variation of the simulated flow depths 1 cm upstream of the buttress tip for $Q = 70$ L/s. This figure gives an idea of how much the flow area variation among the gates depends on the configuration. The results for C7 and C9 were predictable using the one of C6; therefore, they were excluded from this graph to reduce overlapping of the curves in the graph. C8 is a highly nonuniform configuration with low weirs and flow contraction upstream. This configuration led to highly nonuniform distribution of the streamwise accelerations in the lateral direction, and the water surface level varies almost 3 cm there between the 7th and the 8th gates. C6 developed moderate lateral water level variations, as did C7 and C9. Configurations C4 and C5 have the smallest differences in the flow depths because of the low nonuniformity in their geometries. The results confirm that the 1D model assumptions hold, resulting in a successful prediction of the flow rates. In Fig. 8, the deviations of the flow depth due to stagnation pressure rise at the buttress tips are observable and driving the local flow contraction per gate.

The quantification of the lateral flow was achieved by calculating the net lateral flow rate over the weir crests by using the simulated velocity field. First, the absolute value of the cell y-velocities (U_y) was calculated. They were integrated over their respective flow area (the area over the weir crest with normal vector in x-direction) to estimate the absolute lateral flow rate (Q_y) as $Q_y = \int |U_y| dA$. The streamwise area was selected due to its direct and uniform effect over the weir capacity. The sum of the lateral flow rates for each notch gives the total absolute lateral flow rate. This sum was divided by the total streamwise flow rate (Q_x) to estimate a dimensionless lateral flow rate term as follows:

$$Q_L^* = \frac{\sum Q_y}{Q_x} \tag{9}$$

Q_L^* values were estimated at each numerically tested case (36 cases total) separately. The variation of Q_L^* with configuration

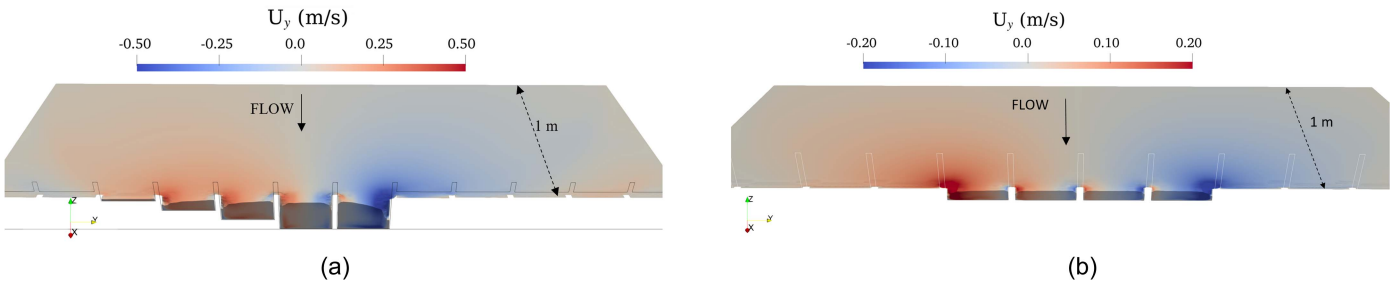

Fig. 7. Lateral velocity (U_y) variations at the surface from the weir extending 1 m upstream of it connected to a vertical section over the weir for: (a) C8 when $Q = 70$ L/s; and (b) C7 when $Q = 20$ L/s.

J. Hydraul. Eng., 2025, 151(4): 04025013

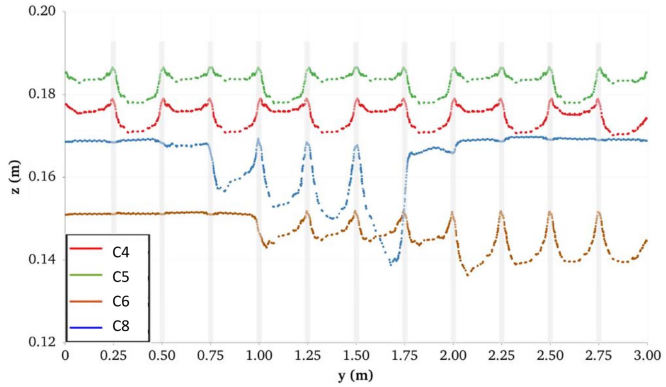

Fig. 8. Variation of the simulated water surface levels at a lateral section 1 cm upstream of the buttress tip for all configurations with $Q = 70$ L/s (the gray vertical background bars indicate the 2-cm-thick buttress locations).

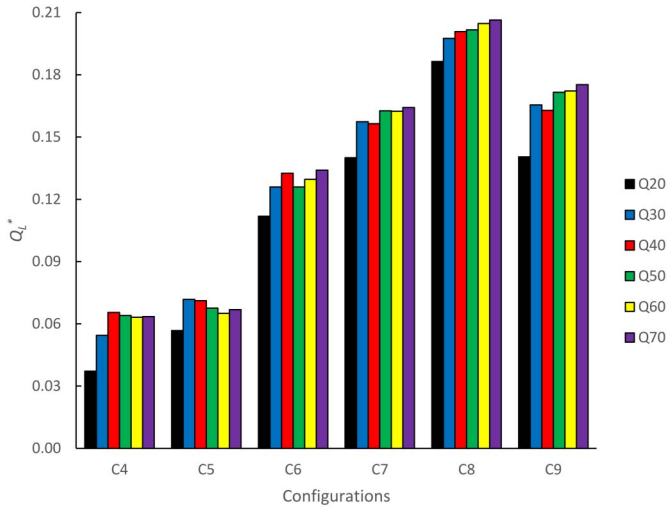

Fig. 9. Variation of Q_L^* by configuration and flow rate. The bars at each configuration show Q_L^* values from the lowest to highest tested discharge.

at each flow rate is shown in Fig. 9. The effect of configuration change on Q_L^* is significant. The largest Q_L^* is always observed at C8, which is the most nonuniform geometry and results in the highest deviations in 1D model results. The deviations of the 1D model results when applied to configurations C9, C7, and C6 were smaller, which resulted in smaller values of Q_L^* compared to C8. C4 and C5 have much smaller Q_L^* values than the ones for C6 to C9. For these configurations, the 1D model already predicted the flow rates successfully. The results reveal that the overestimations at the 1D model formula are correlated to and most likely due to the neglected effects of the horizontal flow contraction. The smallest flow rate (20 L/s) gives a different Q_L^* behavior than the other flow rates, as some flowing notches become nonflowing, and the effected geometry of the weir changes. At C4, this happens at 30 L/s.

Although Q_L^* can be used to quantify the lateral flow magnitude, it requires 3D simulation results that cannot be estimated by using the 1D model results. Although it is not easy to model this kind of highly multidimensional flow by using a 1D approach, we proposed a new parameter that can be used instead of Q_L^* under

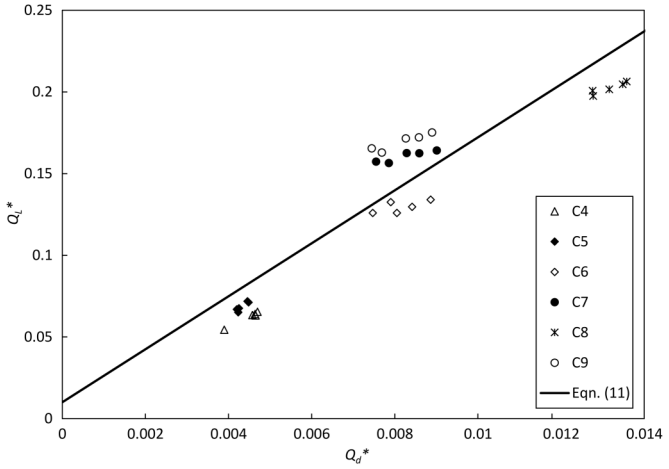

Fig. 10. Variation of Q_d^* and Q_L^* at each case, excluding the $Q = 20$ L/s cases.

the conditions tested in this study. When the lateral flow, and thus the flow contraction, increases, the variance in the streamwise flow rate over the compound weir gates increases. The standard deviation of the estimated flow rates over each gate $\left[\sigma = \sqrt{\frac{\sum_{i=1}^{N}(Q_i - \overline{Q})^2}{N}}\right]$ shows the variance of the flow rates through notches and was used to establish the new parameter. We observed that σ depends on the upstream flow depth, unlike Q_L^*. Therefore, we normalized σ with a discharge term that carries upstream flow depth, h_u, information to estimate the new dimensionless parameter, Q_d^*, as follows:

$$Q_d^* = \frac{\sqrt{\frac{\sum_{i=1}^{N}(Q_i - \overline{Q})^2}{N}}}{Bg^{0.5}h_u^{1.5}} \tag{10}$$

where N is the number of weir openings; Q_i is the flow rate passing through gate i, as predicted by the 1D model; $\overline{Q}$ is the total mean flow rate passing through the gates; B is the total flume width; and g is the gravitational acceleration. Q_d^* values for each tested case were calculated using the measured h_u to eliminate the prediction errors of the CFD model for h_u. Q_i values were obtained from the CFD model. Q_d^* and Q_L^* values were compared (Fig. 10) for each case. An almost linear relation was obtained, which can be defined by using the following simple equation:

$$Q_L^* = 16.22Q_d^* + 0.01 \tag{11}$$

The data were fit to this equation with a high coefficient of determination, $R^2 = 0.86$. The Q_L^* values of C4, C5, C6, and C8 were slightly underestimated using Eq. (11), while that of C7 and C9 were slightly overestimated.

Proposed Correction for the 1D Model Discharge Coefficients

As parameters Q_L^* and Q_d^* are used to quantify the lateral flow, they can now be used to correct the overestimations of the 1D model. The tested discharge case with the flowing notch condition different from the others (20 L/s) was excluded from the analysis. The average Q_L^* values for C6 to C9 are given in Table 1. C4 and C5 require no correction for the 1D model. Their highest Q_L^* value is 0.081 and the lowest one for configurations C6 to C9 is 0.145. We therefore

Table 1. Average Q_L values for the configurations that had significant horizontal flow contraction

Configuration	Average Q_L
C6	0.141
C7	0.173
C8	0.210
C9	0.180

consider roughly that the 1D model discharge coefficients to be corrected if Q_L^* is greater than 0.1.

Using the average values given in Table 1, a new discharge coefficient, C_L, for correcting the 1D model against the lateral flow is proposed such that $Q_{\text{corr.}} = C_L \times Q$, where Q is the discharge obtained using Eq. (1) and $Q_{\text{corr.}}$ is the corrected discharge. The new C_L parameter is given as

$$C_L = 1 - Q_L^* \tag{12}$$

which according to Eq. (11) equals

$$C_L = 0.99 - 16.22 Q_d^* \tag{13}$$

Following the condition defined earlier, the correction of the discharge coefficient is valid if C_L is less than 0.9. Eq. (13) can now be implemented into the 1D model. It requires an iterative search due to the necessity to include both the flow depth and discharge in the formulation. The whole procedure to be applied in the application of the 1D analytical model is summarized in Fig. 11 as a flowchart of the model. The convergence graphs of C_L for each tested case are given in the Supplemental Materials.

Fig. 12 compares the corrected 1D model results with the experimental data. After the correction for horizontal flow contraction, the model predicts the flow rates with high accuracy. The maximum deviation from the measurement was observed as 9.7% at the lowest discharge case of configuration C2. The mean of the absolute deviations from the measurements was 2.45%. The less accurately predicted flow rate was 20 L/s, with a mean of 4.75% deviation from the measurements, which is understandable as Q_L^* values at this flow rate were diverging from the others due to the change in the flowing notch conditions.

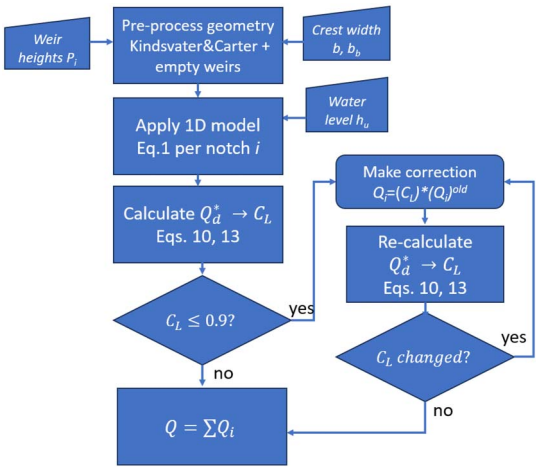

Fig. 11. Summary of the 1D analytical model application.

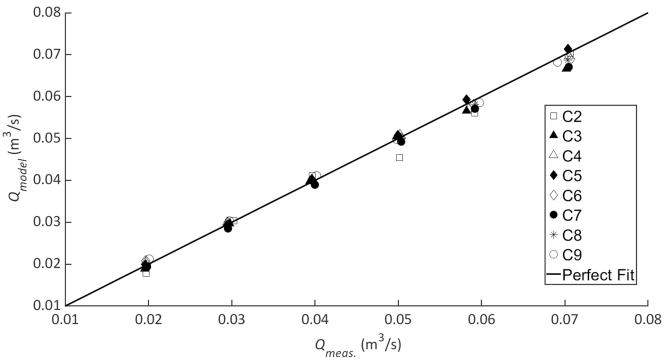

Fig. 12. Comparison of flow rates obtained from the corrected 1D analytical model [Eq. (13)] and experimental data.

Validation Tests for the Proposed Empty Weir Coefficient

For configuration C8, the assigned empty weir discharge coefficient of 0.66 worked well within the discharge range tested in the experimental part of this study. To check whether this accuracy is preserved at higher discharge values, supplementary CFD simulations were conducted using inflowing discharge values of 100 L/s, 150 L/s, 200 L/s, 250 L/s, and 300 L/s. Fig. 13 shows the comparison of the flow depth predictions of the 1D and CFD models. The measured values are also given within the range of the experiments. Besides the corrected 1D model results, uncorrected 1D model results are given for comparison. The corrected 1D model predicts the measured or CFD simulated flow depths successfully at almost all discharge values tested. Diverging behavior is observed at the highest two discharge values (250 L/s and 300 L/s). The overestimations in the 1D model results suggest that the model overestimates the resistance the weir offers to the flow. This may be due to the need for an increase in the empty weir discharge coefficient as the flow depth increases. As the flow depth rises, the relative resistance effect of the weir on the flow decreases, leading to a necessity of increase in the weir discharge coefficient. Further discussions on this result can be found under the subheading "Evaluation of Model Results against Literature Data." Fig. 13 also shows the large underestimations of the uncorrected 1D model. Coincidentally, uncorrected model results get closer to the CFD

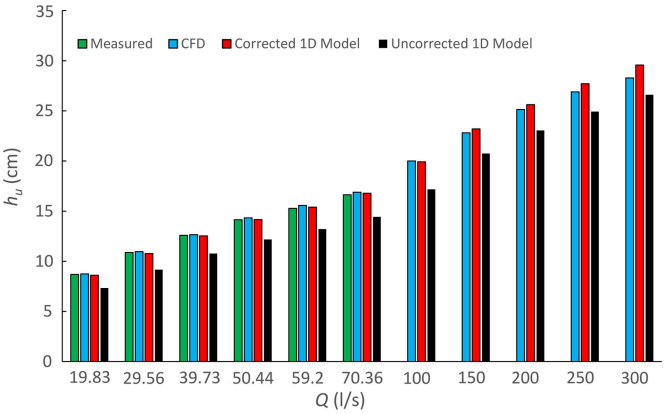

Fig. 13. Comparison of measured h_u values with the analytically and numerically simulated ones for C8 at various Q values including higher flow rates beyond the range of the experiments.

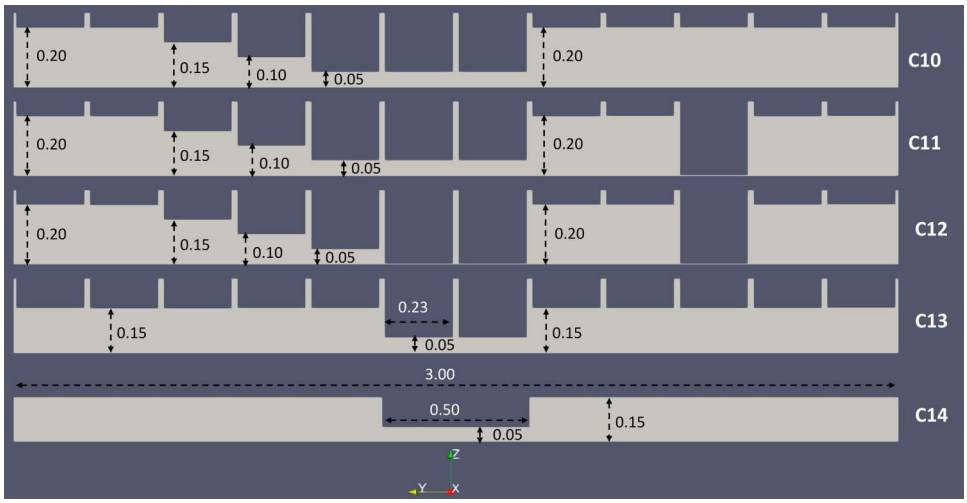

Fig. 14. Weir geometries designed for additional tests. The top three represent nonuniform geometries, while the lower two were used to further analyze insights from the data of Jan et al. (2006) (all dimensions in m).

results at high discharges with the effect of low empty weir discharge coefficients.

Evaluating the Performance of the Proposed 1D Model with Diverse Non-Uniform Configurations

The performance of the 1D model was tested using three more highly nonuniform weir geometries (C10, C11, and C12 in Fig. 14). An inlet discharge range beyond the capacity of the experimental conditions was selected extending to 100 L/s. These cases were simulated using the CFD model, and the resulting upstream flow depths from the CFD model were used as inputs for the 1D model to solve for the flow rates. The results obtained with the 1D model were then compared with the inlet discharges of the CFD model, as shown in Fig. 15. The errors in the model predictions for each configuration were within the acceptable 10% error limit. Due to the nonuniform geometries, all cases required C_L corrections. The uncorrected model results, represented by lighter symbols in Fig. 15, highlight the necessity and effectiveness of the correction when compared to the corrected results.

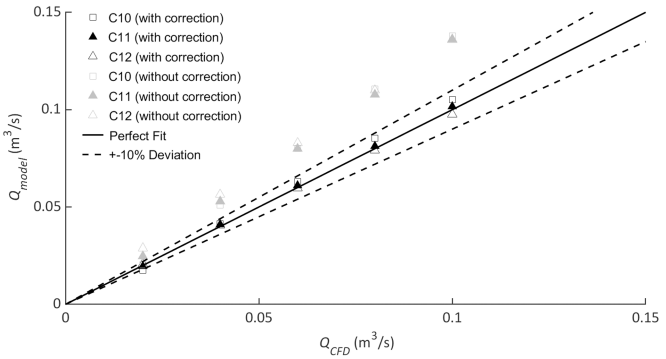

Fig. 15. Comparison of flow rates from the 1D analytical model and CFD simulations for sets C10 to C12. Black markers represent corrected model results, while gray markers indicate uncorrected model results.

Evaluation of Model Results against Literature Data

The literature is very scarce in terms of experimental data sets for rectangular sharp-crested compound weirs. Therefore, we tested the performance of the proposed model by using the only data set that is available (Jan et al. 2006). In that study, rectangular sharp-crested compound weir geometries with varying dimensions and flow conditions were used (Fig. 16 and Table 2). In these geometries, no buttresses were used, making them substantially different from those in our study in terms of lateral flow magnitudes, given the buttresses' known effect of interrupting lateral flow. To model these configurations, the weir crest was divided into equal lengths and each segment was treated as a separate notch. The comparison of the modeled and the measured flow rates is given in Fig. 17.

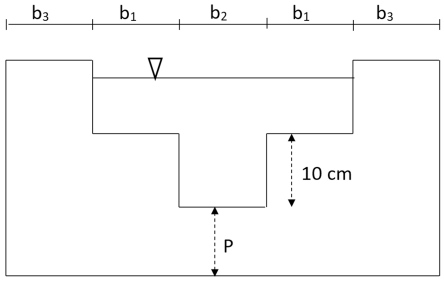

Fig. 16. Schematic of the compound weir section used in Jan et al. (2006). (Reprinted from Jan et al. 2006, © ASCE.)

In cases RR1 to RR6, weirs had end contractions and a single lowered portion at the center. For cases RR1 to RR3, the end contraction was significant with $b/B = 0.47$, while in the remaining cases, b/B was 0.80. The effect of end contraction was accounted for using the Kindsvater and Carter approach. The weir crest's lowered portion comprised 28% of the total crest length in cases RR1 to RR3, and 17% in cases RR4 to RR6. The nonuniformity of the geometry was low in terms of weir crest level change, so no corrections were needed for cases RR1 to RR3, and only minor corrections ($C_L = 0.89$) were required for cases RR4 to RR6. The corrected model's predictions were accurate, with a maximum deviation of 5% from the measurements.

In cases RR7 to RR12, there was no end contraction, and the weir crest had only one lowered portion at the center, accounting for 40% of the weir length. This increased the nonuniformity of the

Table 2. Test conditions of Jan et al. (2006)

Run number	b_1 (cm)	b_2 (cm)	b_3 (cm)	P (cm)	Q (L/s)
RR1 to RR3	25	20	39.5	8	14.63, 16.33, 19.20
RR4 to RR6	50	20	14.5	8	14.63, 16.33, 19.20
RR7 to RR12	40	20	0	11	14.75, 24.65, 36.60, 47.30, 57.70, 75.30

Note: Dimensions refer to Fig. 16.

geometry. In the model application, the corrections were used; i.e., C_L values were smaller than 0.9 because of the variety in the flow rates over the weir portions. The model accurately predicted the data for the lowest flow rate, while the uncorrected model overestimated it. However, as the tested flow rate increased, the model began to underestimate the flow, with deviations from measurements growing alongside the flow rate. Conversely, the uncorrected model's results started to align more closely with the data at higher flow rates. In this set, high flow rates led to significant flow depths due to small flume width. The flow depths over the top of the weir ranged from 1.1 cm to 8.8 cm, increasing with the flow rate. In the present study, we did not test such high flows over nonuniform geometries. As the flow depth over the weir increases, the effect of weir geometry on the flow gets smaller, reducing the effect of lateral flow at high flows. Given the smaller flume width used in that study, the effect was more pronounced. This effect is also observed at Fig. 13 when testing the model performance by using CFD simulations. As the flow rate, and thus the flow depth over the weir, increased, the corrected model started to deviate from the reference values and the uncorrected model results started to align more closely with them. Consequently, the variation in flow rates over each portion of the weir is expected to decrease as they become more uniform. However, the drop in variance was insufficient due to the relatively high level difference (10 cm) between the lowered and remaining portions of the weir crests, which developed a considerable difference between the flow rates among the weir portions. The 1D model's estimated C_L values, based on the variance of the flow depths between the weir portions, were 0.755 and 0.734 at the smallest and highest tested discharges, respectively. The results suggest the need to define a new limiting value for the 1D model, considering the flow depth over the highest elevation of the weir.

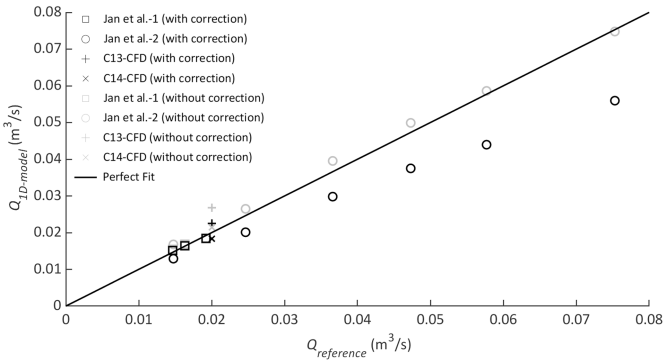

Fig. 17. Comparison of flow rates between the 1D analytical model and measurements from Jan et al. (2006), as well as the CFD model results for cases C13 and C14. The x-axis represents measured flow rates for comparison with Jan et al. (2006) and CFD-simulated results for the rest. Black markers represent corrected model results, while gray markers indicate uncorrected model results.

The Effect of Buttresses on the Flow Rate Capacity of the Weirs

The compound weir used in the study of Jan et al. (2006) did not have any buttresses, which differs from the geometries used in the present study. Although the model successfully predicted the measured flow rates at low flow depths, its ability could not be tested using a variety of weir configurations without buttresses. To demonstrate the effect of buttresses on the flow, a limited numerical assessment was conducted. Two new weir geometries, configurations C13 and C14, were designed to closely resemble those used by Jan et al. (2006), as shown in Fig. 14. The geometry included a long crest and a lowered small notch, as applied in Jan et al. (2006). The flume width was kept the same, making the weir crest length of C14 8% longer than that of C13.

Both CFD simulations were performed using an inflow discharge of 20 L/s. This relatively small discharge was selected to remain within the domain capacity of previous cases and use the same developed mesh. The inflow discharge was introduced as the inlet boundary condition for the CFD models. Then, the upstream flow depths were estimated from their results. These flow depths were used as the inputs of the 1D model to predict the flow rates. The obtained results are compared in Fig. 17. The uncorrected 1D model results are also shown using lighter symbols.

The corrected and uncorrected model results of C14, which has no buttresses, align well with the data of Jan et al. (2006). However, for C13, the corrected model result is closer to the reference value than the uncorrected one, indicating a need of correction. The CFD model estimated a higher flow depth for C13 compared to C14 at the same flow rates, meaning that C13 has less flow rate capacity than C14 for the same upstream flow depths. This indicates that the weir geometries with and without buttresses would not behave the same under the same inflowing discharges.

The lateral flow estimated for C14 was substantially larger than for C13, as the buttresses in C13 partially blocked the lateral flow. The estimated Q_L^* magnitudes from the CFD analysis were 0.2229 for C14 and 0.1295 for C13. For C13, the estimated Q_L^* value was slightly lower than the one calculated using Eq. (11), while for C14, it was considerably higher. Therefore, to apply the outcomes of this study to weirs without buttresses, Eq. (11) should be recalibrated.

Conclusion

The flow over sharp-crested rectangular compound weirs was analyzed under free-flow conditions to establish a reliable 1D approach for flow rate calculations. Eight weir configurations were examined in the physical experiments, covering a range of geometries from uniform to nonuniform and asymmetric. At the same flow rate, the highest upstream flow depths were observed at the configuration with the largest weir area (C3) and at the one with the highest nonuniformity in geometry (C8). The well-known Kindsvater and Carter approach was used as the basis for the 1D model to estimate flow rates from known upstream flow depths. The correction parameter of this method for weir crest width, K_b, was calibrated to account for the addition of buttresses and should be tested again under different conditions. The Kindsvater and Carter approach includes a reduction in the flow rate due to the horizontal contraction of the flume at the weir section. However, some compound weirs experience horizontal flow contraction due to the uneven heights of neighboring weir notches, which does not require an end contraction to develop. The Kindsvater and Carter approach fails to quantify this effect on flow rate accurately. In this study, we incorporated the flow rate reducing effect of this type of flow contraction into the 1D model. The uncorrected 1D model predicted flow rates with

high accuracy for uniform to slightly nonuniform weir geometries. To develop a correction method for significantly nonuniform weirs that cause substantial horizontal flow contraction, CFD analysis results were used. The horizontal flow contraction due to nonuniform weir geometries was quantified using lateral velocities over the weir, which were then related to the standard deviation of the flow rates over each weir notch. A new weir discharge coefficient correction (C_L) for nonuniform weir geometries was defined. This correction can be obtained using the 1D model results without running the CFD model. The corrected model provided acceptable predictions, with a maximum deviation of 9.7% and a mean deviation of 2.45% in flow rate predictions across all 48 cases tested. For the empty gates of one tested configuration, a constant weir coefficient, $C_d = 0.66$, was used. This value was found acceptable within the tested flow rate range in the physical experiments. To check the robustness of the approach, CFD simulations were conducted up to more than 4 times the maximum flow rate tested in the physical experiments. Though the overall results were acceptable, the selected empty weir C_d value seems to need an increase for the highest discharge values. This adjustment is necessary because the rising flow depth over the weir reduces the relative effect of the weir on resistance compared to low flow depth cases. The performance of the proposed model was tested using three additional highly nonuniform configurations. The model performed well, predicting the discharge capacities at the 15 associated cases within a 10% error range.

Additionally, the model's performance was evaluated using another study's experimental results, which involved symmetrical sections without buttresses among the notches. For these geometries, the model accurately predicted the weir discharge capacity at low flow rates but underestimated it as the flow rate and thus flow depth over the crest increased. Consequently, the model's application range was limited to low flows over the weir. However, a limiting factor could not be defined with the lack of validation tests. To demonstrate the effect of buttresses on flow, two more CFD simulations were conducted. The distinct behavior of these two conditions in terms of lateral flow development was observed. Therefore, a new relation, similar to Eq. (11), is essential for accurately representing compound weirs without buttresses.

Data Availability Statement

The code that supports the findings of this study is available in the GitHub repository at https://github.com/burhanyildiz/SharpCrestedCompoundWeirFreeFlowDischargeModel. This code was made available in accordance with the funder data retention policies.

Acknowledgments

The project was supported by the Dutch Ministry of Public Works (Rijkswaterstaat), case 31147818. Part of the works of B.Y. were funded by TUBITAK (Program No: 2219) of Türkiye. The authors acknowledge the use of computational resources of the DelftBlue supercomputer, provided by Delft High Performance Computing Centre (https://www.tudelft.nl/dhpc).

Supplemental Materials

There are supplemental materials associated with this paper online in the ASCE Library (www.ascelibrary.org).

References

Al-Khatib, I. A., and M. Gogus. 2014. "Prediction models for discharge estimation in rectangular compound broad-crested weirs." *Flow Meas. Instrum.* 36 (Apr): 1–8. https://doi.org/10.1016/j.flowmeasinst.2014.01.001.

Altan-Sakarya, A. B., M. A. Kokpinar, and A. Duru. 2020. "Numerical modelling of contracted sharp-crested weirs and combined weir and gate systems." *Irrig. Drain.* 69 (4): 854–864. https://doi.org/10.1002/ird.2468.

Bos, M. G. 1989. *Discharge measurement structures*. Wageningen, Netherlands: International Institute for Land Reclamation and Improvement.

Boussinesq, J. 1877. *Essai sur la théorie des eaux courantes*. Paris: Impr. Nationale.

Clemmens, A. J., T. L. Wahl, M. G. Bos, and J. A. Replogle. 2001. *Water measurement with flumes and weirs*. Rep. No. 58. Wageningen, Netherlands: International Institute for Land Reclamation and Improvement.

Emiroglu, M. E., N. Kaya, and H. Agaccioglu. 2010. "Discharge capacity of labyrinth side weir located on a straight channel." *J. Irrig. Drain. Eng.* 136 (1): 37–46. https://doi.org/10.1061/(ASCE)IR.1943-4774.0000112.

Esch, T., and F. Menter. 2001. "Elements of industrial heat transfer predictions." In *Proc., 16th Brazilian Congress of Mechanical Engineering (COBEM)*. Berlin: Springer.

Ferdowsi, A., M. Valikhan-Anaraki, S. F. Mousavi, S. Farzin, and S. Mirjalili. 2021. "Developing a model for multi-objective optimization of open channels and labyrinth weirs: Theory and application in Isfahan irrigation networks." *Flow Meas. Instrum.* 80 (Aug): 101971. https://doi.org/10.1016/j.flowmeasinst.2021.101971.

Göğüş, M., Z. Defne, and V. Ozkandemir. 2006. "Broad-crested weirs with rectangular compound cross sections." *J. Irrig. Drain. Eng.* 132 (3): 272–280. https://doi.org/10.1061/(ASCE)0733-9437(2006)132:3(272).

Henderson, F. M. 1966. *Open channel hydraulics*. New York: Macmillan Publishing.

Hirt, C. W., and B. D. Nichols. 1981. "Volume of fluid (VOF) method for the dynamics of free boundaries." *J. Comput. Phys.* 39 (1): 201–225. https://doi.org/10.1016/0021-9991(81)90145-5.

Jan, C.-D., C.-J. Chang, and F.-H. Kuo. 2009. "Experiments on discharge equations of compound broad-crested weirs." *J. Irrig. Drain. Eng.* 135 (4): 511–515. https://doi.org/10.1061/(ASCE)IR.1943-4774.0000019.

Jan, C.-D., C.-J. Chang, and M.-H. Lee. 2006. "Discussion of 'Design and calibration of a compound sharp-crested weir' by J. Martínez, J. Reca, M. T. Morillas, and J. G. López." *J. Hydraul. Eng.* 132 (8): 868–871. https://doi.org/10.1061/(ASCE)0733-9429(2006)132:8(868).

Jiang, L., M. Diao, H. Sun, and Y. Ren. 2018. "Numerical modeling of flow over a rectangular broad-crested weir with a sloped upstream face." *Water* 10 (11): 1663. https://doi.org/10.3390/w10111663.

Kindsvater, C. E., and R. W. Carter. 1957. "Discharge characteristics of rectangular thin-plate weirs." *J. Hydraul. Div.* 83 (6): 1–36. https://doi.org/10.1061/JYCEAJ.0000142.

Kulkarni, K. H., and G. A. Hinge. 2020. "Experimental study for measuring discharge through compound broad crested weir." *Flow Meas. Instrum.* 75 (Oct): 101803. https://doi.org/10.1016/j.flowmeasinst.2020.101803.

Lee, J.-T., H.-C. Chan, C.-K. Huang, and J.-M. Leu. 2012. "Experiments on hydraulic relations for flow over a compound sharp-crested weir." *Int. J. Phys. Sci.* 7 (14): 2229–2237.

Li, S., J. Yang, and A. Ansell. 2021. "Discharge prediction for rectangular sharp-crested weirs by machine learning techniques." *Flow Meas. Instrum.* 79 (Jun): 101931. https://doi.org/10.1016/j.flowmeasinst.2021.101931.

Martinez, J., J. Reca, M. T. Morillas, and J. G. Lopez. 2005. "Design and calibration of a compound sharp-crested weir." *J. Hydraul. Eng.* 131 (2): 112–116. https://doi.org/10.1061/(ASCE)0733-9429(2005)131:2(112).

Menter, F. R., M. Kuntz, and R. Langtry. 2003. "Ten years of industrial experience with the SST turbulence model." *Turbul. Heat Mass Transfer* 4 (1): 625–632.

Nouri, M., P. Sihag, O. Kisi, M. Hemmati, S. Shahid, and R. M. Adnan. 2023. "Prediction of the discharge coefficient in compound broad-crested-weir gate by supervised data mining techniques." *Sustainability* 15 (1): 433. https://doi.org/10.3390/su15010433.

Okagaki, Y., T. Yonomoto, M. Ishigaki, and Y. Hirose. 2021. "Numerical study on an interface compression method for the volume of fluid approach." *Fluids* 6 (2): 80. https://doi.org/10.3390/fluids6020080.

OpenCFD. n.d. "OpenFOAM user guide." Accessed May 28, 2024. https://www.openfoam.com/documentation/user-guide/.

Piratheepan, M., N. E. F. Winston, and K. P. P. Pathirana. 2006. "Discharge measurements in open channels using compound sharp-crested weirs." *J. Inst. Eng. Sri Lanka* 40 (3): 31–38. https://doi.org/10.4038/engineer.v40i3.7144.

Qu, J., A. S. Ramamurthy, R. Tadayon, and Z. Chen. 2009. "Numerical simulation of sharp-crested weir flows." *Can. J. Civ. Eng.* 36 (9): 1530–1534. https://doi.org/10.1139/L09-067.

Rehbock, T. 1929. "Discussion of precise weir measurements by EW Schoder and KB Turner." *Trans. ASCE* 93 (1): 1143–1162.

Rijnwaardense Uiterwaarden. n.d. "Regelwerk Pannerden." Accessed May 28, 2024. http://www.rijnwaardenseuiterwaarden.nl/pages/regelwerk-pannerden.html.

Salmasi, F., G. Yıldırım, A. Masoodi, and P. Parsamehr. 2013. "Predicting discharge coefficient of compound broad-crested weir by using genetic programming (GP) and artificial neural network (ANN) techniques." *Arabian J. Geosci.* 6 (Jul): 2709–2717. https://doi.org/10.1007/s12517-012-0540-7.

Sargison, J. E., and A. Percy. 2009. "Hydraulics of broad-crested weirs with varying side slopes." *J. Irrig. Drain. Eng.* 135 (1): 115–118. https://doi.org/10.1061/(ASCE)0733-9437(2009)135:1(115).

Savage, B. M., B. M. Crookston, and G. S. Paxson. 2016. "Physical and numerical modeling of large headwater ratios for a 15 labyrinth spillway." *J. Hydraul. Eng.* 142 (11): 04016046. https://doi.org/10.1061/(ASCE)HY.1943-7900.0001186.

Swamee, P. K. 1988. "Generalized rectangular weir equations." *J. Hydraul. Eng.* 114 (8): 945–949. https://doi.org/10.1061/(ASCE)0733-9429(1988)114:8(945).

Thielicke, W., and R. Sonntag. 2021. "Particle image velocimetry for MATLAB: Accuracy and enhanced algorithms in PIVlab." *J. Open Res. Software* 9 (1): 12. https://doi.org/10.5334/jors.334.

Torres, C., D. Borman, A. Sleigh, and D. Neeve. 2021. "Application of three-dimensional CFD VOF to characterize free-surface flow over trapezoidal labyrinth weir and spillway." *J. Hydraul. Eng.* 147 (3): 04021002. https://doi.org/10.1061/(ASCE)HY.1943-7900.0001852.

Versteeg, H. K. 2007. *An introduction to computational fluid dynamics the finite volume method, 2/E*. Chennai, India: Pearson Education India.

Wessels, P., and A. Rooseboom. 2009. "Flow-gauging structures in South African rivers Part 1: An overview." *Water SA* 35 (1): 1–9. https://doi.org/10.4314/wsa.v35i1.76643.

Yildiz, B., L. Ambagts, M. F. Yossef, and E. Mosselman. 2024. "Evaluation of different numerical approaches to modeling flood flows over groynes." *Water Resour. Res.* 60 (6): e2023WR036895. https://doi.org/10.1029/2023WR036895.

Yildiz, B., and W. Uijttewaal. 2023. "Experimental analysis of flow over rectangular sharp-crested compound weirs." In *Proc., 40th IAHR World Congress 2023: Rivers-Connecting Mountains and Coasts*. Madrid, Spain: International Association for Hydro-Environment Engineering and Research.

Yildiz, B., W. Uijttewaal, J. Bricker, and E. Mosselman. 2021. "Numerical modelling of flow over sharp-crested rectangular contracted weir." In *Proc., 2nd Int. Symp. on Water System Operations*. Madrid, Spain: International Association for Hydro-Environment Engineering and Research.

Zahiri, A., X. Tang, and H. M. Azamathulla. 2014. "Mathematical modeling of flow discharge over compound sharp-crested weirs." *J. Hydro-Environ. Res.* 8 (3): 194–199. https://doi.org/10.1016/j.jher.2014.01.001.

Zhao, G., P. J. Visser, Y. Ren, and W. S. Uijttewaal. 2015. "Flow hydrodynamics in embankment breach." *J. Hydrodyn.* 27 (6): 835–844. https://doi.org/10.1016/S1001-6058(15)60546-7.